© Universiti Tun Hussein Onn Malaysia Publisher's Office

IJIE

http://penerbit.uthm.edu.my/ojs/index.php/ijie
ISSN : 2229-838X e-ISSN : 2600-7916

The International Journal of Integrated Engineering

An Efficient Design of the Piezoresistive Pressure Sensor Applied for Micro Aerial Vehicle

Anh- Duc Pham[1*], Trieu Khoa Nguyen[2], Hong Hieu Le[3], Phuoc Vinh Dang[1]

[1]Faculty of Mechanical Engineering,
The University of Danang - University of Science and Technology, 54 Nguyen Luong Bang,
Da Nang city, 55000, VIETNAM

[2]Faculty of Mechanical Engineering,
Industrial University of Ho Chi Minh City, 12 Nguyen Van Bao, Ho Chi Minh City, 71408, VIETNAM

[3]HUTECH institute of engineering,
Ho Chi Minh City University of Technology (HUTECH), 475A Dien Bien Phu Street,
Ho Chi Minh City, 72325, VIETNAM

*Corresponding Author

DOI: https://doi.org/10.30880/ijie.2023.15.01.004
Received 15 June 2021; Accepted 27 August 2021; Available online 28 February 2023

Abstract: In this research, the developing process of a piezoresistive pressure sensor working in the atmosphere environment applied in micro aerial vehicle using the MEMS fabrication method is introduced. The sensor consists of four Au/Cr piezoresistors in a Wheatstone bridge configuration on a wet oxidized silicon diaphragm. To fabricate the sensor, three lithographic steps were conducted: the first one is to define the resistors and Au/Cr lines/pads, the second and the third ones are to determine the width and the thickness of the square SiO_2/Si diaphragm, respectively. The sensor diaphragm shape and thickness were defined by the anisotropic etching of Si in tetramethylammonium hydroxide (TMAH) solution, and the resistors array are formed by sputtering and wet etching method. The sensor size is 6000 µm by 6000 µm. The sensor output voltage was measured for various applied pressure levels from -0.9 to 1.2 bar with 5V voltage supply. The fabricated pressure sensor also exhibits a sensitivity of 50.1 mV/bar.

Keywords: Piezoresistive pressure sensor, micro-aerial-vehicle component, atmosphere environment, MEMS

1. Introduction

Micro aerial vehicles (MAV) have attracted great interest in commercial industries as well as academic research around the world [1]. Since their portability enables them to perform a wide range of applications. A Broad Agency Announcement (BAA 97-29) by DARPA in 1997 defined MAV as the vehicle being less than 15 cm in any dimension [2]. Due to their small size and light weight, it is convenient to transport them to a launch site and to be operated by a single operator. This advantage makes them an ideal candidate for missions like investigating hazardous level in space-confined areas [3]. It is also very difficult to visibly detect them with their compact size, hence, MAVs are suitable for surveillance missions [4]. These are just few examples of missions or application that MAV can conduct. On the other hand, the fabrication of such small size vehicles requires new research in designing optimization procedures, inventing lightweight materials, fabricating microelectronic devices, and so on [5-6]. Among the microelectronic devices required for MAV, barometric pressure sensor is an important one and thus the pressure sensor in this work is designed for a range of 0-1.2 bar.

Microelectromechanical system (MEMS) is a system where mechanical, and electronics elements are integrated in a common substrate using integrated circuit process techniques [7-9]. With the advantages of MEMS technology,

*Corresponding author: ducpham@dut.udn.vn

devices or systems can be fabricated with tiny sizes and are capable of sensing, controlling and operating at the micro-scale but they can result in macro-scale effects [8]. This technique is a well-known candidate for the batch fabrication of sensors [10-11]. Physical quantities such as vibrations, mechanical properties, magnetic fields, and temperatures in systems are sometimes difficult to detect by conventional sensors, which are often unwieldy and sizeable [12]. Therefore, microsensors can be applied to easily identify those quantities and the changes of the surrounding environment on the system. Upon receiving that information, Microelectronic components in those sensors process it and command integrated micro-actuators to perform actions corresponding to those changes in the environment. For example, MEMS sensors have been applied in IoT based step monitoring systems owing to their low-power consumption [11].

Among the successful devices fabricated by MEMS technique, pressure sensors are one of the most successful MEMS based devices [13]. MEMS pressure sensors have been greatly interested since they are useful in numerous applications including health care [14], automobiles [15-16], and aerospace applications [17] and so on. MEMS pressure sensors detect the pressure level by generating an electrical signal output proportional to the applied pressure. Up to now, there are five standard transduction mechanisms used for pressure sensing are piezoresistive, capacitive, piezoelectric, optical, and resonant pressure sensing [18-20]. Among mentioned transduction mechanisms for MEMS pressure sensors, piezoresistive and capacitive mechanism have been mostly used.

The working principle of piezoresistive and capacitive pressure sensor is based on the deflections of an elastic diaphragm caused by pressure variations in the media such as gases or liquids [21-23]. The bending of the diaphragm induces the mechanical changes at the diaphragm, which are then measured by piezoresistive or capacitive techniques. Although capacitive pressure sensors have higher pressure sensitivity and lower temperature dependence, their main disadvantages are non-linearity and signal loss from stray capacitance. On the other hand, piezoresistive pressure sensors were more widely used as they have higher linearity, compact size, simple readout circuit, fast response time and so on. Furthermore, in the list of sensing materials used for piezoresistive pressure sensor, metal based piezoresistors have the advantage of simple construction and durability through sputtering or vacuum evaporation techniques, compared to other more complicated and expensive fabrication method like diffusion or ion implantation. Hence, up to date piezoresistive pressure sensors are still being used and fabricated to be adapted in many pressure sensing applications, not only in MAV systems but also in the integrated board used for the unmanned aerial vehicle (UAV) systems [24-25]. In the context of this study, the aim is to fabricate a sensor with a compact size, which is not too small and with a simple readout circuit. These desirable characteristics of the sensor leads to the simplicity of the fabrication technique, which makes the sensor fabrication scalable.

In this paper, the simple design and fabrication of a pressure sensor using the piezoresistive effect is illustrated. The proposed pressure sensor consists of a deformable diaphragm and Au/Cr electrodes-integrated piezoresistors array configured in a Wheatstone bridge. Different applied pressure levels are detected from the variation in the output voltage of the Wheatstone configuration. The proposed pressure sensor has a sensitivity of approximately 50.1 mV/bar and extremely suitable for working in the atmosphere environment. The fabrication process involves three photolithography steps and two etching steps. Moreover, the testing process of this fabricated pressure sensor is illustrated in the sections of experiment and results. By using MEMS technique, we have achieved the sensor with the size compact enough to be integrated on MAV and proved the scalability of the fabrication method.

2. Structural Design of the Piezoresistive Pressure Sensor

2.1 Geometrical Design

Figure 1 illustrates the schematic structure of the pressure sensor. In particular, it consists of a SiO_2/Si diaphragm with 4 piezoresistors located along its edges and Au/Cr contact layer. The overall size of the sensor is 6000 µm × 6000 µm, and the SiO_2/Si diaphragm is 5000 µm × 5000 µm with the thickness of 40 µm. Every piezoresistors consists of 14 small strips with the thickness of 0.11 µm, the width of 40 µm, and the length of 650 µm. Four square Au/Cr electrodes located at four corners of the diaphragm have the dimensions of 1500 µm by 1500 µm. The resistance of piezoresistors can be varied by the displacement of the diaphragm subject to different applied pressures. Figure 1(b) illustrates the cross-sectional views of the pressure sensor. The cavity of the pressure sensor has a slanted wall due to the anisotropic etching of TMAH, which is discussed in more details in the section 2.2.

To analysis the strain distribution through the diaphragm due to the ambient pressure, a commercial finite element analysis (FEA) program—COMSOL Multiphysics—was used. The simulated parameters are presented in Table 1. The diaphragm edges were clamped, and this was considered as boundary condition in the simulation. Fig. 2 shows the simulation results of the diaphragm displacement under the applied pressure ranging from 0 to 1.2 bar. As shown in Fig. 2(a), the pressure centre is located at the centre of the square diaphragm. More importantly, the maximum stress occurs at the edge of the diaphragm. Thus, the placements of piezoresistors have to be as close as possible to these locations to maximize the effect of the strain on the piezoresistors. As seen by the simulation results, the diaphragm displacement is linearly proportional to the applied pressure as illustrated in Fig 2(b). Therefore, it is expected that the linearity of the diaphragm displacement results in the linearity of the output voltage of the fabricated pressure sensor.

Table 1 - Simulation parameter for the designed pressure sensor

Parameter	Units	Value
Density	kg/m^3	2330
Young modulus	GPa	160
Poison ratio	-	0.2

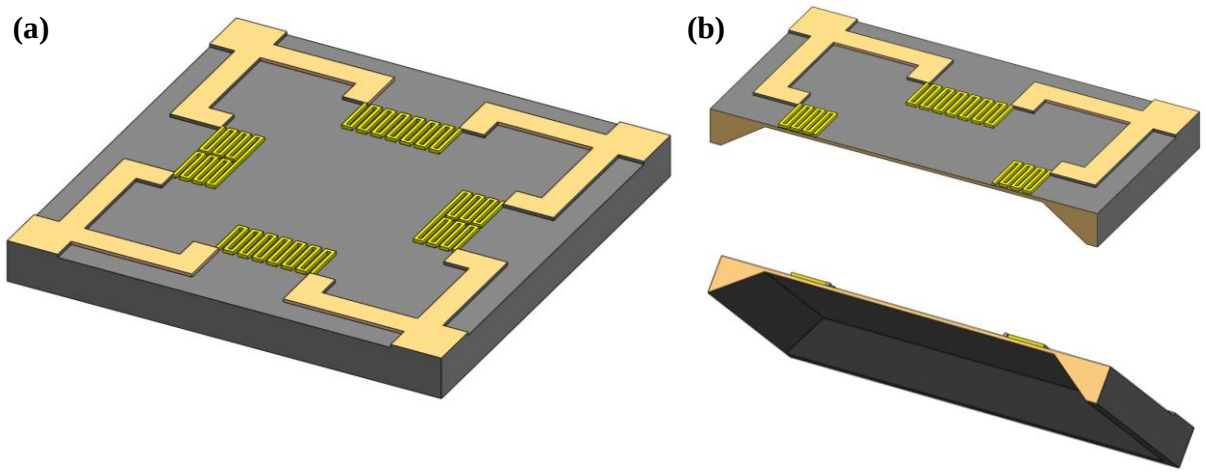

Fig. 1 - The schematic diagram of the designed pressure sensor (a) structure of the designed sensor and; (b) half cross-section of sensor

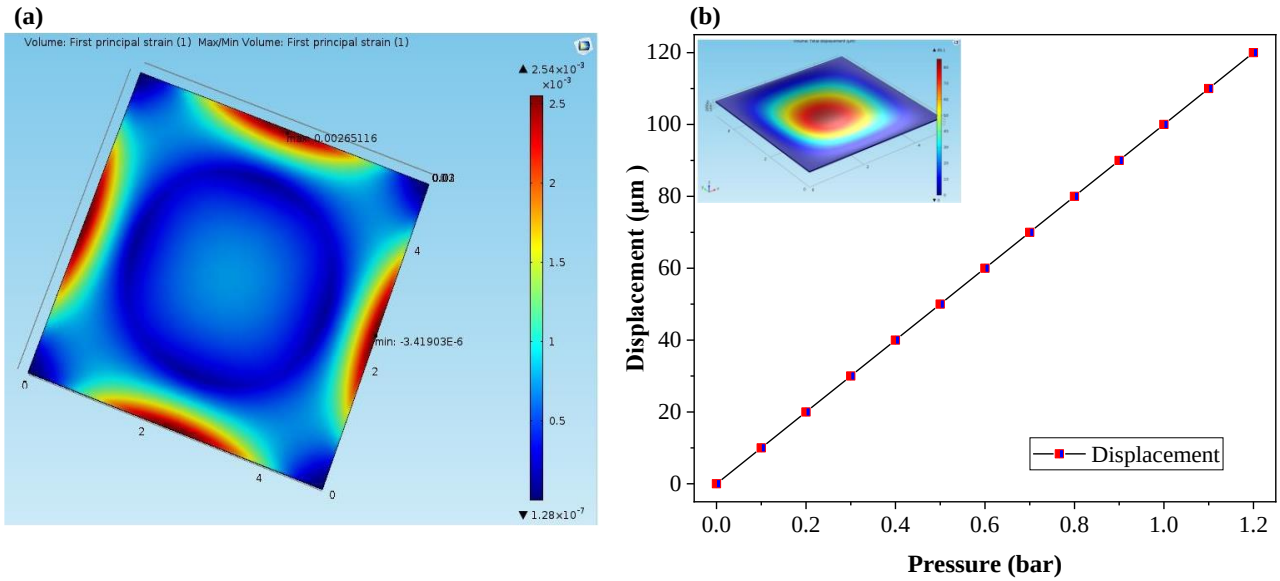

Fig. 2 - FEA of silicon diaphragm showing (a) stress distribution on the diaphragm and; (b) its displacement as a linear function of applied pressure

Figure 3(a) shows the operational principle for the pressure level sensor. When pressure is applied to the sensor diaphragm, the diaphragm deformation is proportional to the amount of pressure applied. It can be seen that the piezoresistors configuration forms a Wheatstone bridge. Initially, all the resistors have the same resistance, and the bridge is considered as balanced, which results in zero output voltage. When the sensor diaphragm is subjected to stress, its edges experience strains, which are transferred to the resistors. Therefore, resistors undergo change in dimensions and consequently their resistance also change. These changes in resistance make the bridge unbalanced and produce an output voltage, which is proportional to the external applied stress. To discuss in more details how this principle is specifically applied in our case, Fig. 3(b) presents the sensor top view with the piezoresistor and contact pad. It can be observed that the top and bottom resistors - R1 and R4 - have the same geometries. Similarly, the left and right resistor-R2 and R3-are also designed the same. Every piezoresistor consists of 14 small strips and each strip has the thickness of 0.11 µm, the width (W) of 40 µm, and the length (L) of 650 µm. Hence, without any applied pressure, their initial resistances are the same. Under pressure applied to the diaphragm, the lengths of R1 and R4 become longer,

increasing their total resistance. Meanwhile, the widths of R2 and R3 becomes wider, their cross- sectional area increase, reducing their total resistance. Therefore, this leads to the unbalance of the Wheatstone bridge. Since in our case, all piezoresistors have the same dimensions, only different geometries, the output voltage of our fabricated sensor is computed by using the following equation [26].

$$V_{out} = V_{in}\left(\frac{R_1}{R_1+R_2} - \frac{R_3}{R_3+R_4}\right) = V_{in}\frac{\Delta R}{R} \quad (1)$$

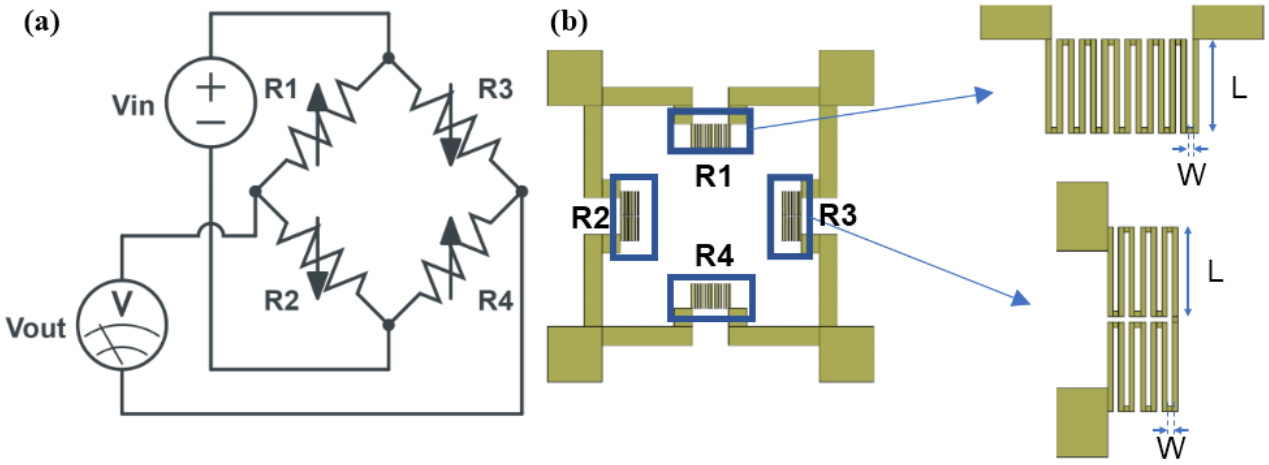

Fig. 3 - Principle of the pressure sensor (a) operational principle for the pressure level sensor and; (b) top view of resistors arrays configured as the Wheatstone bridge

2.2 Fabrication of The Piezoresistive Pressure Sensor

The process flow for fabrication of the designed sensor is shown in Fig. 4 and consisted of the following steps: (a) 4-inch (100) p-type Si single side polished wafers were cleaned using RCA process and thermally wet oxidized to form a 400 nm-thick SiO_2 layer on both sides of the wafer, which was used as a layer for shallow etching of silicon. (b) A 10-nm layer of Cr was sputtered onto the sample to increase the adhesion of Au and subsequently a 110-nm layer of Au was formed, (c) Au/Cr film was coated with photoresist, then the first photolithographic and etching step was performed to define the piezoresistors. (d) The front side SiO_2 layer was selectively removed using the second photolithography step and etching with buffered hydrofluoric acid (BHF). (e) With SiO_2 as a masking layer and using TMAH solution at 80 ºC, Si etching was carried out on the front surface of wafer to achieve a target depth of 40 µm, which is the thickness of the diaphragm. (f) The backside of the wafer was coated with photoresist and the third photolithographic step was performed to selectively etching SiO_2, (g) Finally, the diaphragm was formed by a second time of anisotropic etching of Si in TMAH solution at 80 ºC. Finally, we achieved the structure of the piezoresistive pressure sensor.

3. Experiment and Results

Figure 5(a) illustrates the schematic diagram of the experimental setup for measuring the diaphragm displacement of the sensor and its corresponding output voltages as a function of different levels of applied pressure. An 5V input voltage was provided to the sensor by a DC power supply. The pressure was applied to the sensor diaphragm by using a motorized syringe driver connected to a lab made 3D printed jig. The motorized syringe can move forward and backward to apply the positive and negative pressures, respectively. In particular, when the syringe moved forward, the air was injected into the sealed chamber, the positive gauge pressures applied led to the upward deflection of the silicon diaphragm. On the other hand, when the syringe moved backward, the air was drawn out of the chamber and the diaphragm was bent downward by the negative gauge pressures. A digital pressure gauge was also connected to monitor the applied pressure level. The deflection at the diaphragm centre was measured by using a 10-nm resolution laser vibrometer. The output voltage was measured using a source meter.

Figure 5(b) is the photograph of the setup for characterising the performance of the as-fabricated pressure sensor. The entire setup was placed on an anti-vibration table to ensures that external vibrations do not affect our measurement results. All the measurements are conducted in the clean room with the temperature of 20°C and the humidity of ~35%. The pressure was attached to a lab-made 3D printed jig as show in the top image.

To determine the mechanical hysteresis of the sensor, the sensor diaphragm was subject to various pressures under two cycles: testing and recovery as shown in Fig. 6. For measuring the positive gauge pressures, the testing cycle is the

process in which the applied pressure is first increased by steps of 0.1 bar and the recovery cycle is the process in which the applied pressure is decreased by steps of 0.1 bar. For measuring the negative gauge pressures, the testing cycle is the process in which the applied pressure is first decreased by steps of 0.1 bar and the recovery cycle is the process in which the applied pressure is increased by steps of 0.1 bar.

In Fig. 7 and 8, the testing and recovery cycles are depicted by the thick solid red curve and the short dash blue curve, respectively. Figure 7 (a, b) demonstrates the graph of the diaphragm displacement corresponding to various applied positive and negative gauge pressures, respectively. It is clear that the displacement of the silicon diaphragm is almost a linear function of applied pressure. Figures 7(c, d) show the output voltage as a function of various applied pressure values at standard laboratory conditions. It is clear that two curves of testing and recovery cycles are almost identical. Hence, the fabricated sensor has a very minimal mechanical hysteresis.

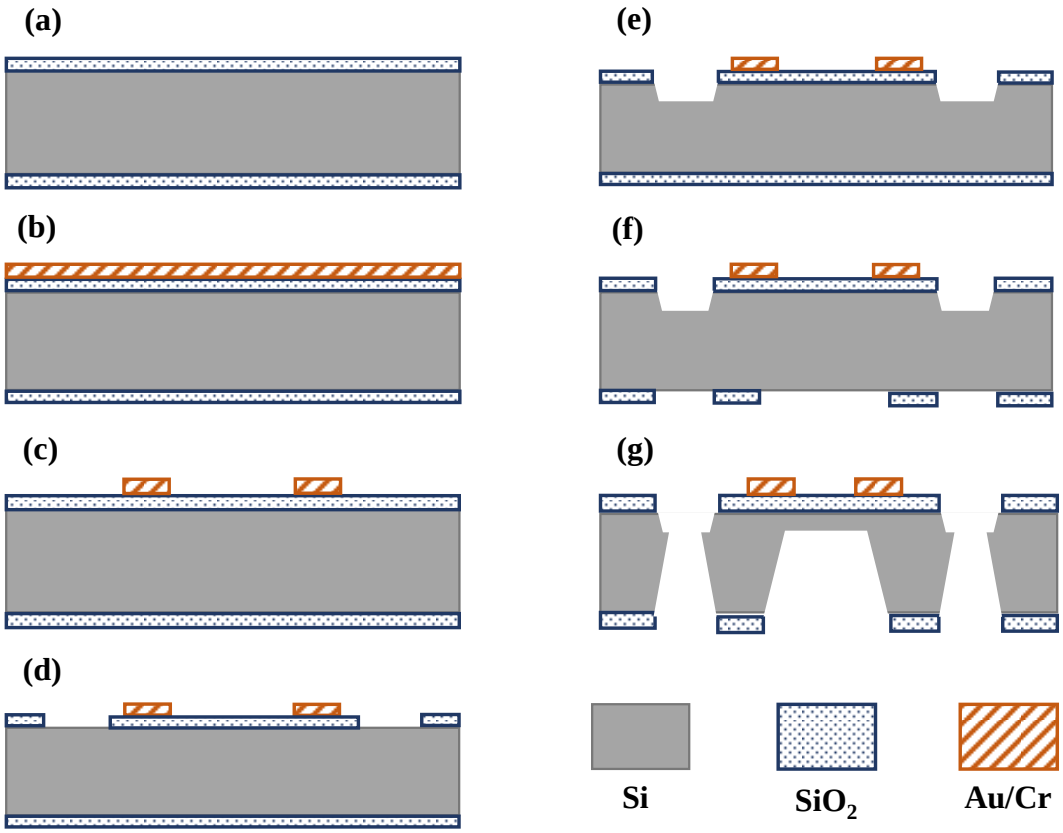

Fig. 4 - The fabrication process flow of the pressure sensor (a) SiO_2 growth; (b) Au/Cr deposition; (c) Au/Cr etching; (d) topside SiO_2 etching; (e) topside Si etching; (f) backside SiO_2 etching and; (g) backside Si etching

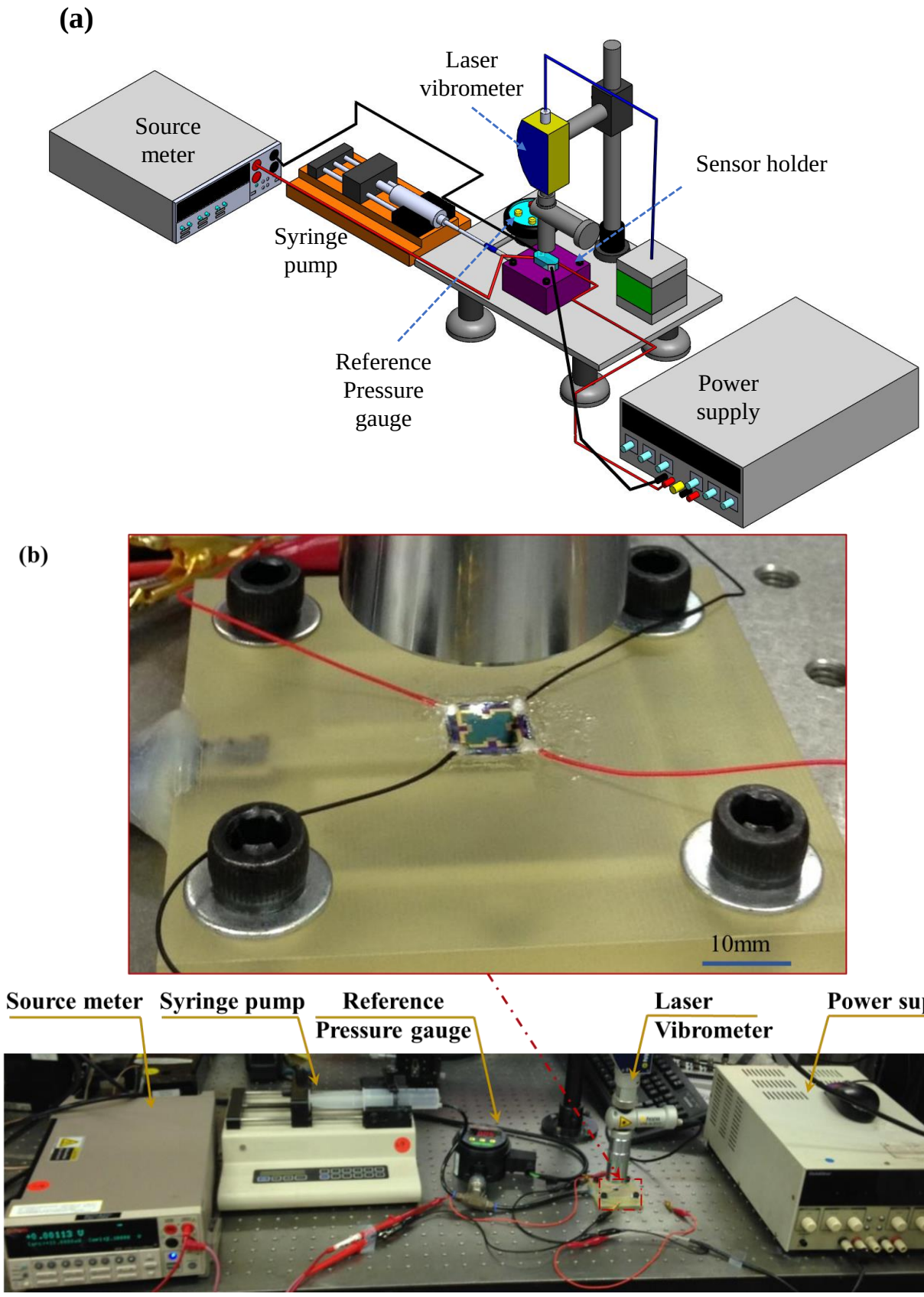

Fig. 5 - Experiment of piezoresistive pressure sensor applied in MAV (a) the schematic illustration and; (b) the image of the experimental setup to measure diaphragm displacement of the sensor and its corresponding output voltages (Magnified photograph is the fabricated pressure sensor attached to a jig)

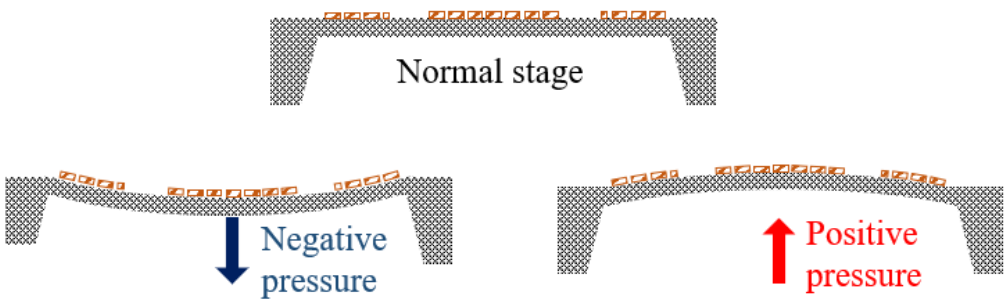

Fig. 6 - Testing process for the fabricated pressure sensor

The fabricated sensors have an offset voltage of about 51.6 mV, which can be diminished by using extra resistors on the sensors. This offset voltage can result from the geometry error during the sensor fabrication. The sensitivity of the fabricated sensor is approximately 50.1 mV/bar.

Considering the resistivity, the thickness, the length, and the width of the piezoresistors, their initial resistance in the bridge is 90 Ω. The change in resistance of the resistors is calculated using Eq. (1) and presented in Fig. 8(a). Figure 8(b) shows the ratio between the change in the resistance and the initial resistance. Similar to Fig. 7, the testing and recovery cycle cures also follow each other. Furthermore, all specification of the designed pressure sensor is illustrated in Table 2.

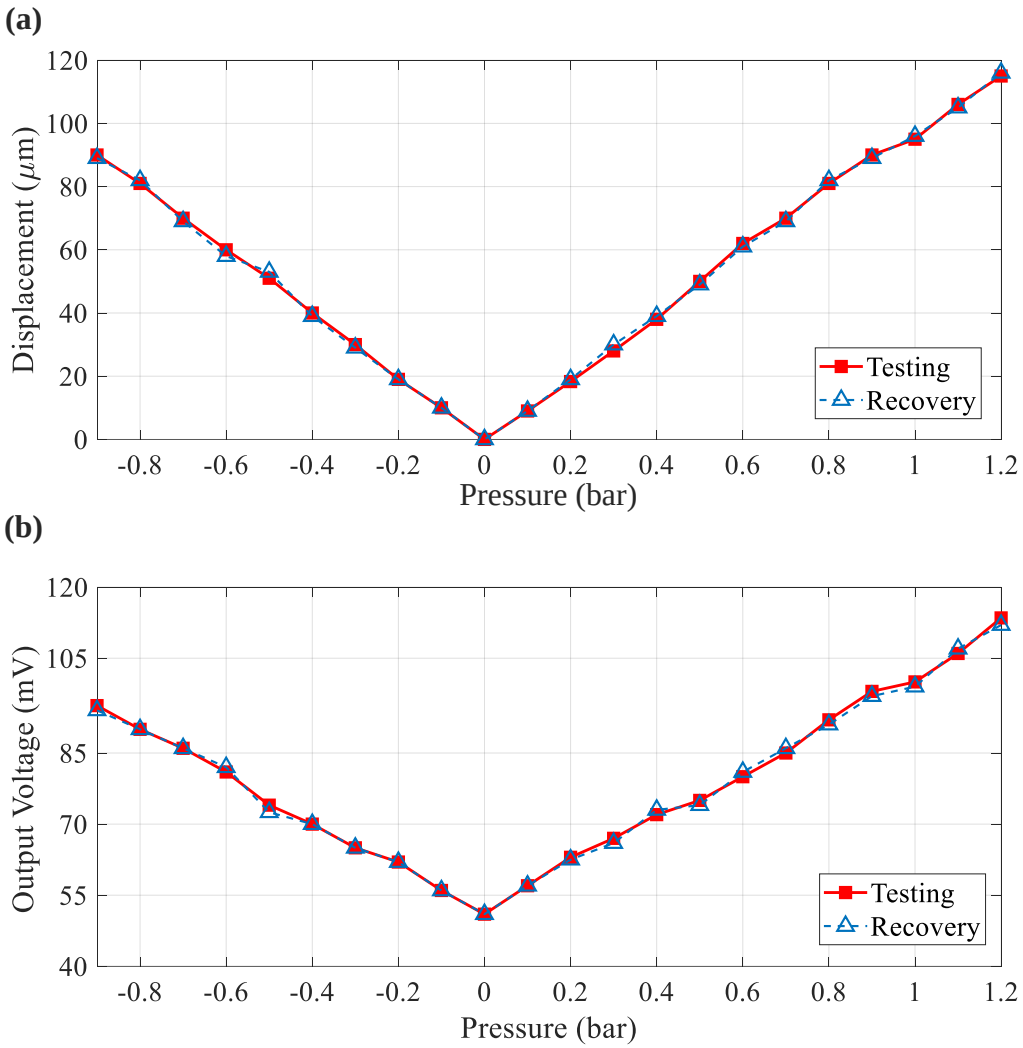

Fig. 7 - Correlation between sensor's responses and input pressure (a) the diaphragm displacement and; (b) the sensor output voltage as a function of pressure

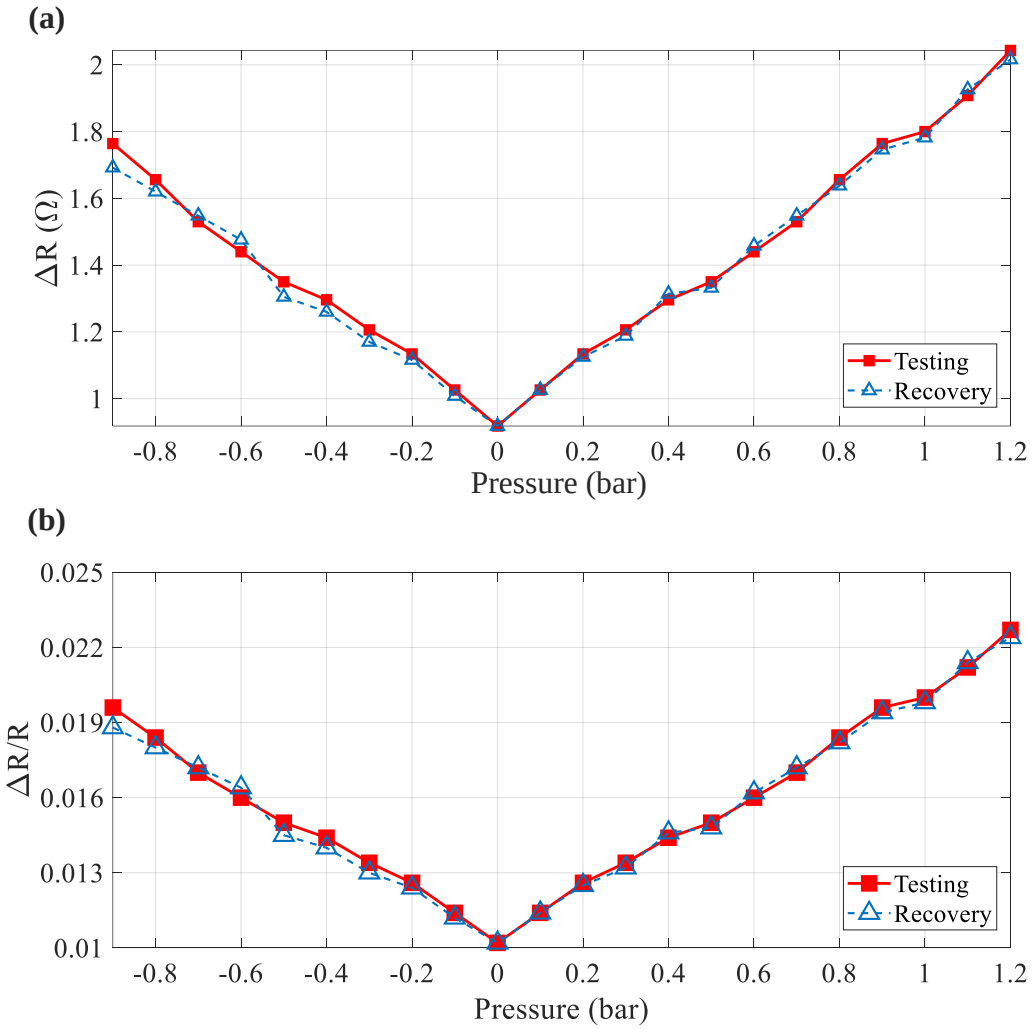

Fig. 8 - Correlation between the internal resistor of Wheatstone bridge and input pressure (a) change in the resistance and; (b) the ratio of ΔR/R as a function of applied pressure

Table 2 - Specification of the fabricated pressure sensor

Parameter	Unit	Value
Dimension	µm×µm	6000×6000
Input voltage	V	5
Zero output	mV	51.6
Full range output	mV	113.5
Sensitivity	mV/bar	50.1
Gauge pressure	bar	-0.9÷1.2

4. Conclusion

In this work, authors designed and fabricated a piezoresistive pressure sensor that measures pressure change by using voltage output change of a piezoresistor array configured in a Wheatstone bridge. The structure of the diaphragm and the placement position of the piezoresistors were optimized by using a commercial FEA software package-COMSOL Multiphysics and fabricated by MEMS processes. Experimental results confirmed that the sensor output voltage is almost a linear function of the varying pressure in the range of -0.9÷1.2 bar, which makes it suitable to be integrated into MAV operating in the atmospheric environment. The simulation and experimental results are consistent with each other, and experimental results confirmed that the sensitivity of sensor is approximately 50.1 mV/bar.

The fabricated sensor with the dimension of 6000µm by 6000µm is compact enough making it suitable for being integrated in the MAV. Moreover, by taking advantage of MEMS technique, the possibility of the scalable production of the fabricated pressure sensor has been demonstrated.

Acknowledgement

This work was supported by The University of Danang, University of Science and Technology, code number of Project: No. T2021-02-28.

References

[1] Ward, T. A., Fearday, C. J., Salami, E., & Binti Soin, N. (2017). A bibliometric review of progress in micro air vehicle research. International Journal of Micro Air Vehicles, 9(2), 146-165.

[2] Sivasankaran, P. N., Ward, T. A., Viyapuri, R., & Johan, M. R. (2016). Static strength analysis of dragonfly inspired wings for biomimetic micro aerial vehicles. Chinese Journal of Aeronautics, 29(2), 411-423. https://doi.org/10.1016/j.cja.2016.02.007

[3] Deshpande, M. D., Sivapragasam, M., & Umesh, S. (2020). An efficient miniature air suction system for chemical sensors for micro air vehicle application. Sādhanā, 45(1), 116. https://doi.org/10.1007/s12046-020-01352-y

[4] Ng, T. T. H., & Leng, G. S. B. (2002). Application of genetic algorithms to conceptual design of a micro-air vehicle. Engineering Applications of Artificial Intelligence, 15(5), 439-445.

[5] Michelson, R. C. (2010). Overview of Micro Air Vehicle System Design and Integration Issues. In Encyclopedia of Aerospace Engineering. John Wiley & Sons, Ltd. https://doi.org/10.1002/9780470686652.eae401

[6] Mieloszyk, J, Galiński, C. (2013). Assessment of the concept of a propeller working in a slot in the middle of wing of a micro air vehicle. Archive of Mechanical Engineering, 60(2), pp. 269-282.

[7] R. Ghodssi and P. Lin. (2011). MEMS materials and processes handbook. In New York: Springer. https://doi.org/10.5860/CHOICE.49-0882

[8] [8] Nafea, M., Schlosser, C., Kazi, S., Mohamed, Z., Mohamed Ali, M. S. (2017). Optimal Two-Degree-of-Freedom Control for Precise Positioning of a Piezo-Actuated Stage. Int. J. of Integrated Eng. -Special Issue on Electrical Electronic Engineering, 9(4), 93-102.

[9] Mazurek, G. (2012). Digital Vibration Sensor Constructed with MEMS Technology. International Journal of Electronics and Telecommunications, 58(2), 117-122. https://doi.org/ 10.2478/v10177-012-0016-4

[10] Rahimi, Z., Yazdani, J., Hatami, H., Sumelka, W., Baleanu, D., Najafi, S. (2020). Determination of hazardous metal ions in the water with resonant MEMS biosensor frequency shift - concept and preliminary theoretical analysis". Bulletin of the Polish Academy of Sciences: Technical Sciences, 68(3), 529-537.

[11] Chow, K-D., Abdal-Kadhim, A. M, Kok, S. L., Lau., K-T. (2019). Finite Elements Method Simulation of P(VDF-TrFE) Piezoelectric Sensor for Internet of Things Application. Int. J. of Integrated Eng., 11(1), 77-83. https://doi.org/10.30880/ijie.2019.11.01.010.

[12] Le, H.N., Dang, P.V., Pham, A-D., Vo, N.T. (2020). System identifications of a 2DOF pendulum controlled by QUBE-servo and its unwanted oscillation factors. Archive of Mechanical Engineering,67 (4), 435-450.

[13] Bryzek, J., Roundy, S., Bircumshaw, B., Chung, C., Castellino, K., Stetter, J. R., & Vestel, M. (2006). Marvelous MEMs. IEEE Circuits and Devices Magazine. https://doi.org/10.1109/mcd.2006.1615241

[14] Zang, Y., Zhang, F., Di, C., & Zhu, D. (2015). Advances of flexible pressure sensors toward artificial intelligence and health care applications. Materials Horizons, 2(2), 140-156. https://doi.org/10.1039/C4MH00147H

[15] Wang, J., Xia, X., & Li, X. (2012). Monolithic Integration of Pressure Plus Acceleration Composite TPMS Sensors With a Single-Sided Micromachining Technology. Journal of Microelectromechanical Systems, 21(2), 284-293. https://doi.org/10.1109/JMEMS.2011.2178117

[16] Gryś, S. (2019). An experimental test bench for the tire pressure monitoring system - Discussion of measurement and communication issues. Int. J. of Electronics and Telecommunications. https://doi.org/10.24425/123565

[17] Lin, L., & Yun, W. (1998). MEMS pressure sensors for aerospace applications. IEEE Aerospace Conference Proceedings. https://doi.org/10.1109/AERO.1998.686941

[18] Javed, Y., Mansoor, M., & Shah, I. A. (2019). A review of principles of MEMS pressure sensing with its aerospace applications. Sensor Review, 39(5), 652-664. https://doi.org/10.1108/SR-06-2018-0135

[19] Belavič, D., Bradeško, A., Zarnik, M. S., & Rojac, T. (2015). Construction Of A Piezoelectric-Based Resonance Ceramic Pressure Sensor Designed For High-Temperature Applications. Metrology and Measurement Systems, 22(3), 331-340. https://doi.org/10.1515/mms-2015-0034

[20] Anand, A. Pal, Kundu, S. (2021). Bandwidth and Power Enhancement in the MEMS Based Piezoelectric Energy Harvester using Magnetic Tip Mass. Bulletin of the Polish Academy of Sciences: Technical Sciences, e137509, 1-8. https://doi.org/0.24425/bpasts.2021.137509

[21] Mishra, R. B., El-Atab, N., Hussain, A. M., & Hussain, M. M. (2021). Recent Progress on Flexible Capacitive Pressure Sensors: From Design and Materials to Applications. Advanced Materials Technologies, 6(4), 2001023. https://doi.org/10.1002/admt.202001023

[22] Eaton, W. P., & Smith, J. H. (1997). Micromachined pressure sensors: review and recent developments. Smart Materials and Structures, 6(5), 530-539. https://doi.org/10.1088/0964-1726/6/5/004

[23] Tykhan, M., Ivakhiv, O., & Teslyuk, V. (2017). New type of Piezoresistive Pressure Sensors for Environments with Rapidly Changing Temperature. Metrology and Measurement Systems, 24(1), 185-192.

https://doi.org/10.1515/mms-2017-0010
[24] Eltayeb, A., Rahmat, M. F., Basri, M. A. M. (2020). Adaptive Feedback Linearization Controller for Stabilization of Quadrotor UAV, Int. J. of Integrated Eng.,12(4), 1-17. https://doi.org/10.30880/ijie.2020.12.04.001
[25] Rasib, A. W., Mohd Ali, H., Alvin, L., Kanniah, K., Idris, N. H., Omar, H., Faidi, A., Dollah, R., & Anjang Ahmad, M. (2018). Upscaling Aboveground Biomass Estimation at Low-land Royal Belum Forest Reserve Using Unmanned Aerial Vehicle Image. Int. J. of Integrated Eng., 10(4), 140-150.
[26] Morgenshtein, A., Sudakov-Boreysha, L., Dinnar, U., Jakobson, C. G., & Nemirovsky, Y. (2004). Wheatstone-Bridge readout interface for ISFET/REFET applications. Sensors and Actuators B: Chemical, 98(1), 18-27. https://doi.org/10.1016/j.snb.2003.07.017